Modeling Earthquake-induced Landslide initiation using the Fibre Bundle Model

Y. Chen [1*], B. van den Bout [1], L. Lombardo [1], C. J. van Westen [1]

’ corresponding author mail y.chen-6@utwente.nl PO Box 217, Enschede, AE 7500, Netherlands

Abstract

Co-seismic landslides are triggered by strong ground shaking in mountainous areas, resulting in threats to human activity and infrastructure. Methods for physically-based modelling of co-seismic landslide triggering play an important role in disaster prevention and mitigation. Current approaches, however, focus on direct and full failure of sloping rocks and soils, and do not cover the dynamics of partial damage and post-earthquake stability. In order to specify the seismic effect and simulate the dynamic failure process, we propose the use of Fibre Bundle Model (FBM), a mathematical framework to simulate the highly nonlinear behaviour of the progressive damage and breakdown of disordered media statistically. Soil on slopes are considered as bundles of fibres with a certain strength probability distribution. The damage in soil structure gradually increment during ground shaking. Our approach, integrating seismic forcing into the method, allows for prediction of partial damage, as well as full failure. We reach good validation results (AUC of 0.78). Due to the underlying principles, the partial damage can be interpreted as a deterministic partial damage, or as a proxy for failure probability. The partial damage could be critical in predicting the impact of post-seismic landslide effects.

Authorship Contribution statement Y. Chen: Conceptualization, data collection, model development, data processing, data analysis, writing. B. van den Bout: Conceptualization, model development, data processing, writing. L. Lombardo: Conceptualization, data collection, data processing, writing. C. J. van Westen: Conceptualization, writing.

Keywords: Co-seismic landslide; Physically based model; Fibre bundle model

[1] University of Twente, Faculty of Geo-Information Science and Earth Observation (ITC), PO Box 217, Enschede, AE 7500, Netherlands

1 Introduction

Co-seismic landslides triggered by strong earthquakes are the important earthquake effects (Fan *et al.*, 2019). Co-seismic landslides are a significant cause of economic loss and casualties in mountainous areas located in seismically active areas. Their occurrence shows a strong correlation with the intensity of ground acceleration during an earthquake, they can obstruct rivers and reservoirs, and the landslide deposits on slopes can be remobilized during subsequent heavy precipitation and convert into a debris flow.

Numerous studies have been carried out into the different aspects of co-seismic landslides. Geographic Information System (GIS) and remote sensing are used for the generation of co-seismic landslide inventories (Süzen and Doyuran, 2004; Xu *et al.*, 2014), which are essential for understanding the relationship between landslides and their contributing and triggering factors. An open repository for hosting digital inventories is available on the platform of U.S. Geological Survey Science Base (Tanyaş *et al.*, 2017). Factors such as seismic moment, focal depth, and focal mechanism and fault rupture length are generally considered for statistical correlation with landslide locations, and a globally constant threshold of acceleration was also adopted for onset of systematic mass wasting (Marc *et al.*, 2017). Landslide densities are highest in the area with the largest ground acceleration and decrease with distance from the epicentre (Meunier *et al.*, 2007). Amplification of seismic waves associated with convexity in mountain ridges results in higher landslide densities close to ridge crests (Meunier *et al.*, 2008). Next to the density of occurrence, the size and type of landslides are key components for landslide hazard assessment (Lari *et al.*, 2014). These variables are linked to ground movement, distance from the seismic source, local relief, lithology and structural geological context (Valagussa *et al.*, 2019).

Analyzing the susceptibility of landslides is a crucial part of assessing landslide risks (Van Westen *et al.*, 2008). For the aspect of earthquake-induced landslides, several solutions of co-seismic landslide risk assessment have been conducted by many researchers during the past decades. Therefore, a number of useful methods and models are being developed to advance the modelling of the susceptibility of co-seismic landslides. There are a variety of approaches based on statistics and physics. For methods involving statistics, tools such as classical statistics, index based, machine leaning, multi criteria and neural networks are widely used for susceptibility analysis over the past three decades (Reichenbach *et al.*, 2018). New innovations allowed the spatio-temporal prediction of the density of landslides, their surface area and their enumeration in comprehensive Bayesian models. For example, Lombardo and Mai (2018) proposed a work-flow to unify the way the community shares Logistic Regression results for landslide susceptibility purposes, which used the Least Absolute Shrinkage Selection Operator (LASSO) for simultaneous parameter estimation and variable selection in generalized linear models.

Physical-based approaches are based on the physics of the hydrological and geological processes, which use physically based equations that can be beneficial to certain types of applications. For areas with accurate data and limited dynamics, such as floods, accuracy is usually higher than empirical methods. In addition, physically based models predict full dynamics and all involved physical quantities, thus improving the understanding of the processes involved. Finally, these models allow for the exploration of possible scenarios, such as climate change, land use practices or the construction of protective measures. When applied to landslides, physically based models quantify the effect of geotechnical and hydrological parameters on the slope instability based on laws derived from physical principles. Foe example, Newmark's method allows the modelling of a landslide as a rigid friction block that slides on a sloping plane when subjected to a basic acceleration (Newmark, 1965). Subsequent improvements included vertical accelerations, which proved to be significant (Ingles *et al.*, 2006). A regression model on the basis of the Newmark analysis was conducted for regional landslide hazard assessment (Jibson, 2007). The Scoops3D model can incorporate the seismic effect in a pseudo-static model through adding a specified pseudo-acceleration, which is a uniform horizontal coefficient as a fraction of the magnitude of the gravitational acceleration (Reid *et al.*, 2015). Lastly, the OpenLISEM model uses the peak ground acceleration parallel to the direction of the steepest slope in an infinite slope model(Bout *et al.*, 2018).

The existing models for predicting landslides are normally evaluated by considering the presence and absence of landslides, which could be overly simple for reflecting the earthquake effect on a specific slope. To illustrate this, four basic situations of slopes under an earthquake could occur (Figure 1): undamaged slopes, slopes with internal deformation, surface failure, and failed slopes. From a perspective of internal damage, it is very often difficult to differentiate the first and second situation in the field, the second situation may be very close to the third one but the slope has not failed, the third situation could further develop to be the fourth situation after ground shaking. Thus, the typical approaches lead to a big uncertainty in the perspective of mechanisms. Cohen *et al.* (2009) proposed the use of Fiber Bundle Model (FBM) (Peirce, 1926) to simulate the progressive failure of cracks and shear zones in soils for the rainfall-induced landslides. Lehmann and Or (2012) extended the application of FBM for hydro-mechanical triggering landslides, and simulated the process of soil on hillsloe from progressive local failures to mass release. The studies lead to the dynamic process of the landslide triggering mechanisms. Currently, no work exist that includes seismic effect into the FBM method, and analyses its predictions of co-seismic effects. Therefore, we proposed a model framework that combines the FBM and seismic loads to estimate co-seismic slope stability, and to quantify the internal damage of soil under seismic and precipitation disturbances.

2 Modeling strategy

2.1 Evaluation of Force Equilibrium

The modelling approach developed through integrating the infinite slope model and the Fibre Bundle Model (FBM) was used to quantify and present the seismic effects on slopes

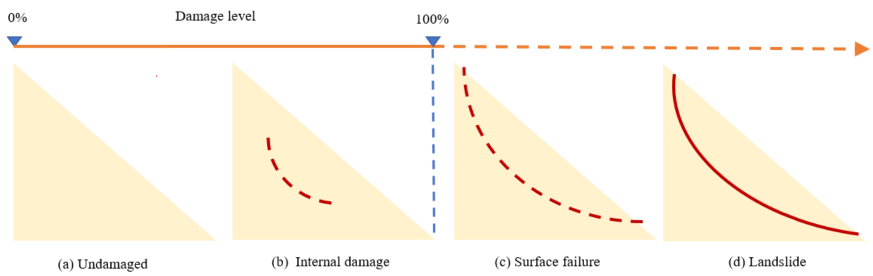

Figure 1: The schematic diagram of earthquake damage effect on slopes. (a) an undamaged slope, (b) a slope with internal damage, (c) surface failure, (d) landslide.

spatially. In this model, the soil on a hillslope is designed to be an assembly of soil columns (See Figure 2). The shear mechanical bonds of soils and the bedrock are considered as virtual fiber bundles, and each bundle contains 10,000 fibres. The slip surface is assumed to be the interface between the soil and bedrock or the interface between the two soil layers. The local force model is used to describe the resisting force and driving forces. The driving force includes a part of weight and the seismic loading. The resisting components consist of capillarity, cohesion, and friction which mainly depended on the local geological and hydrological conditions. The strength of each fibre is derived from the resisting strength of the soil column, when the driving forces applied on fibres,and exceed the critical resistant of fibres, then gradually breaking among fibres happens until all fibres break or reach equilibrium in the soil column. Complete failure of the fibre bundle indicates landslide occurence.

The driving force D and resisting force τ_s are given as

$$D = H_{sd}[\theta\rho_w + (1-\phi)\rho_r]g\cos\beta\sin\beta + H_{sd}\rho_r\alpha\cos\beta^2 \tag{1}$$

$$\tau_s = C_{soil} + \{H_{sd}[\theta\rho_w + (1-\phi)\rho_r]g\cos\beta^2 - \tau_h\}\tan\gamma - H_{sd}\rho_w\alpha\cos\beta\sin\beta\tan\gamma \tag{2}$$

with soil depth H_{sd}, volumetric water content θ, density of water ρ_w, soil porosity ϕ, soil minerals density ρ_r, acceleration due to gravity g, the slope angle along the maximal elevation drop β, soil cohesion C_{soil}, the soil friction angle γ, the soil strength provided by capillary forces τ_h, the peak horizontal acceleration of earthquake α. The seismic forcing in the resisting force formulation is following Morgenstern and Sangrey (1978).

2.1.1 Hydrology

The influence of the spatial and temporal distribution of rainfall on the pore water conditions is an important component of the modelling framework of co-seismic landslides. In order to to model the hydro-logical process in the context of in the rainfall-induced landslides, Lehmann and Or (2012) combined the soil hydrologic parameterization of Brooks and Corey

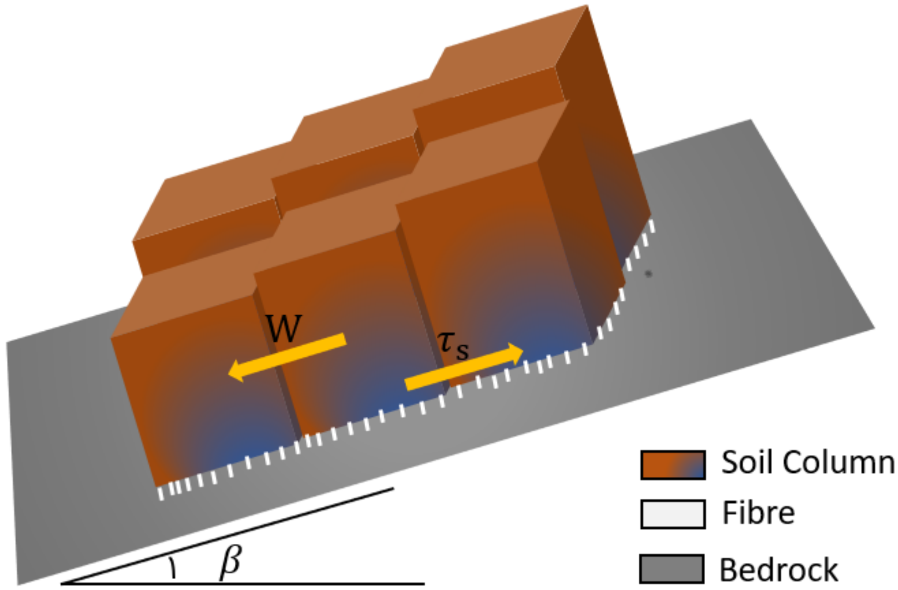

Figure 2: illustration of a hillslope with basic units of square soil columns. Slope angle is β, driving force is D along the down slope direction, shear strength is τ_s along the upslope direction.

(1964) with the formulation for unsaturated soil strength by Lu *et al.* (2010). This model performs well in the hydro-mechanical triggering model framework, and it has been applied in several studies (von Ruette *et al.*, 2013; Fan *et al.*, 2016; Leshchinsky *et al.*, 2021). We have also adopted this hydromechanical model into the modelling framework for co-seismic landslides.

The hydro-logical process considers the infiltration capacity, surface water flow, inter-flow including fast water flow along the soil-bedrock interface, and lateral unsaturated flow within the soil matrix.

with a certain porosity of soil mass, the water content is strongly positively correlated with the weight of soil mass, and hence influences the down-slope driving force, while the intrinsic mechanical strength change negatively. Based on the theory of effective stress of Bishop (1959), soil strength is enhanced proportionally to capillary pressure head h.Lu *et al.* (2010) introduced water saturation Θ as proportion factor linking capillary force with soil strength τ_h. Lehmann and Or (2012) chose the Brooks and Corey (1964) model parameterization for the relationship between water saturation Θ and capillary head h. The soil strength τ_h and other hydraulic properties are given as

$$\tau_h(\theta) = \rho_w g |h_b \Theta^{1-\frac{1}{\lambda}}| \tag{3}$$

$$h_b = 0.042\lambda^{-1.08} \tag{4}$$

$$\Theta = \frac{\theta - \theta_r}{\theta_s - \theta_r} \tag{5}$$

$$\theta_r = 0.01\lambda^{-1.11} \tag{6}$$

with capillary pressure head h, air-entry value h_b, pore size parameter λ, water content θ, effective water saturation Θ, and residual and maximum water content θ_r and θ_s.

The pore size parameter λ is obtained from the soil water characteristic curve based on the Brooks-Corey model, based on the soil texture class. earlier work has shown that the empirical Brooks-Corey model can be derived form fractal modeling of porous media (Friesen and Mikula, 1987; Toledo *et al.*, 1993; Shen and Li, 1994; Shen *et al.*, 1995; Abdassah *et al.*, 1996). Kewen (2004) developed a theoretical model which showed that the pore size parameter λ increases with the decrease in fractal dimension, described by equation

$$\lambda = 3 - D \tag{7}$$

with the fractal dimension. Porous media with greater heterogeneity have smaller values of the pore size parameter λ. Details for the quantification are presented in Appendix A.

2.2 The Fibre Bundle Model

Peirce (1926) first introduced the FBM to study the failure of cotton yarns, which initially consists of a bundle of parallel, elastic, linear fibres of identical length and stiffness stretched almost statically between two plates, either by controlling the deformation or the load (See Figure 3). The FBM is a statistical approach to detect the progressive and dynamic breaking process of materials that have a finite threshold strength pulled at random from a probability density function (PDF). Step loading applied on the bundle causes weak fibres to break, and redistribution of the load between the surviving fibres can trigger cascading breaks. In spite of its simplicity, FBM has proven useful in simulating the highly non-linear behaviour of progressive damage and degradation of disordered media. A systematic introduction is represented by Hansen *et al.* (2015), which involves various applications and the mathematical, computational and statistical backgrounds. For the specific application in landslide modelling, Cohen *et al.* (2009) revealed the strength of the FBM to represent the progressive failure of soils on hill slopes, including soil elements such as interstitial cements, capillarity, frictional contacts, and biological binders. Lehmann and Or (2012) put forward a more complex model framework with FBM to simulate the dynamics of shallow landslides from progressive local failures to mass release, and demonstrated that the size and frequency statistics obeyed power laws with exponents similar to values from real landslide inventories. von Ruette *et al.* (2013) extended the application of the framework for rainfall-triggered shallow landslides at catchment scale, and Fan *et al.* (2015) further revealed the effects of

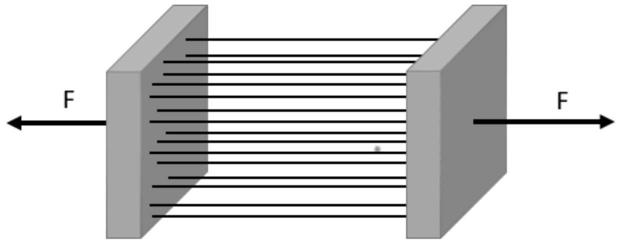

Figure 3: A fibre bundle model stressed by an external force F. A bundle is clamped between two rigid supports. (Hansen *et al.*, 2015)

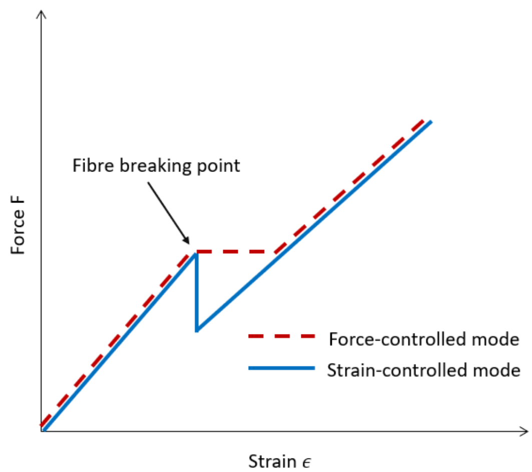

Figure 4: A comparison of the force-controlled mode (red dash line) and the strain-controlled mode (blue solid line). After the breaking of a fibre, the force reduction happens abruptly in strain-controlled mode, while in force controlled mode, the strain increases abruptly due to load redistribution, causing cascading effect within the fibre bundle. (Hansen *et al.*, 2015)

hydromechanical loading history and antecedent soil mechanical damage for subsequent shallow landslides initiation. These studies have demonstrated the ability of FBM for simulating dynamic failure of soils for shallow landslide modelling.

2.2.1 Loading method

A fibre bundle is assumed as a collection of N elastic fibres. When the external force F is applied in the axial direction, the extension of fibres ϵ happens and corresponds with force F. The relationship with a probability distribution $P(\epsilon)$ of fibres is, therefore, $F = N\epsilon(1-p(\epsilon)$, which could be represented in two different mode, strain-controlled with extension ϵ or force controlled mode, with force F as the independent variable.

In the strain-controlled mode, with the increasing of extension x, the decrease of force F happens abruptly due to the rupture of fibres. Therefore there is no load redistribution in the fibre bundle. In contrast, the extension x in the force-controlled situation increases abruptly, further causing global failure of the bundle because of the load redistribution among surviving fibres. We chose the force-controlled mode because the model aims to simulate the dynamics of soil properties with the change of external loading triggered by earthquake and rainfall.

2.2.2 Weibull Distribution for Heterogeneity of Soil Shear Strength

In general, the precise fibre strengths are unknown in soil systems, as it is impossible to measure the strength of soils covering a regional area with sufficient detail. Instead, the probability distributions can be obtained through statistical analysis of soil strength measurements. The probability distribution of fibres strength are essential components of the FBM which plays a critical role for simulating the gradual failure of bundles. The uniform distribution and the two-parameter Weibull distribution are most common used in FBM.

The Weibull distribution was invented by Waloddi Weibull for fatigue testing and analysis (Weibull, 2013), and is also widely applied in reliability engineering, especially for the distribution of cumulative wear failure of electromechanical products. The two-parameter Weibull density distribution (PDF) is given as

$$p(\sigma^{th}) = \frac{m}{k}(\frac{\sigma^{th}}{k})^{m-1} \exp\left[-(\frac{\sigma^{th}}{k})^{m}\right] \tag{8}$$

where σ^{th} is the critial threshold strength of a fibre, m is the shape parameter, and k is the scale parameter. The corresponding cumulative distribution function (CDF) is

$$P(\sigma^{th}) = 1 - \exp\left[-(\frac{\sigma^{th}}{k})^{m}\right] \tag{9}$$

The strengths of soils could be well described by Weibull distribution with different shape parameters m and scale parameters (Lim *et al.*, 2004; Munkholm and Perfect, 2005; Munkholm *et al.*, 2007). Lim *et al.* (2004) presented an analysis of tensile failure of soil grains compressed between flat plates, and demonstrated that this could be represented by a Weibull distribution. (Munkholm and Perfect, 2005) made a comparison of the goodness-of-fit for a three-parameter versus a two-parameter Weibull model, and showed that former fits the aggregate rupture data better. In a further study, Munkholm *et al.* (2007) incorporated the water content in the Weibull Model for Soil Aggregate Strength. The result indicated that the water content had little or no effect on the spread of aggregate strengths.

The shape parameter is one of the key components of the two-parameter Weibull model. Characterising the distribution of defects, it reflects the degree of material strength concentration (Rinne, 2008). With the increase of shape parameter, the strengths are more concentrated, indicating that the brittleness of the soil increases and it is more likely to be damaged, and when shape parameter decreases, the plasticity of the soil increases, which is reflected in the strength enhancement. Gao F (1996) derived the relationship between the fractal dimension and the Weibull modulus based on the hypotheses of the fractal distribution of crack sizes in brittle materials and the weakest link principle. The weakest link principle assumes that weakest elements in a loaded system are the most vulnerable to fail, which is a fundamental hypothesis for modelling the dynamics of failure. Xu *et al.* (2016) conducted a statistical approach describing the evolution of grain fragmentation from mother material to its fragments, which proposed particle fragmentation results in a fractal distribution of progeny fragments, and found a reasonably good relationship between the cumulative survival probability of the particles and the tensile strength following the Weibull distribution. This is a statistical approach based on this discovery, a equation of the Weibull shape parameter and the fractal dimension was formulated as

$$m = \frac{D}{3 - D} \tag{10}$$

with the fractal dimension D (See Appendix A), and m as well as Weibull shape parameter.

The scale parameter k of Weibull distribution is the characteristic value of soil strength, which is the 63.2 percentile of the distribution. It means that for all Weibulls 63.2 percentage of the fibres will fail by a characteristic strength (Weibull, 2013). Cao and Zhang (2005) conducted a research on Weibull analysis of rock damage based on the Mohr-Coulomb criterion, and concluded that the shear strength can be represented by a Weibull probability distribution. Sornette (1989) formulated the relationship of shape parameter m, scale parameter k, and the critical strength of material failure in the context of FBM, by using a central limit theorem, the asymptotic theory of extreme order statistics proposed by Galambos (1978). This study provided a solid method to use the Weibull distribution for the soil strength. Based on Cao and Zhang (2005), and the relationship of Weibull parameters and critical strength from Sornette (1989), we adopted the soil shear strength derived form the infinite slope model as the critical strength of soil to calculate the scale parameter k in our model framework. The equation is givens as

$$k = \frac{\tau_s}{(1/m^{1/m}e^{-1/m})} \tag{11}$$

Where m (right) and k (left) are the Weibull shape and scale parameters, and the τ_s is the critical strength of soil.

2.2.3 Loading Redistribution

Load redistribution between broken and intact fibres starts with breaking of the first fibre, and induces further failures until all remaining fibres can either withstand the load, or until the whole bundle ruptures. The mechanisms of load redistribution vary between two extreme ends: the equal load sharing (ELS) and local load sharing (LLS). The equal load sharing mechanism is the simplest one which assumes that the load from broken fibres is equally distributed to all remaining fibres in case that the supports at the two clamped ends are stiff, while the local load sharing mechanism assumes that the load is redistributed to the neighbourhood of a broken fibre, which one of both supports at clamped bundle ends are soft (Hansen *et al.*, 2015). These mechanisms cause different failure behaviour of the fibre bundle system. Cohen *et al.* (2009) conducted a numerical experiment showing that ELS is not influenced by the fibre topology, while LLS can increase the likelihood of catastrophic failure because of the short-range interaction.

For the consideration of softness of soil, the LLS would match the reality better than ELS. Meanwhile, the LLS model depends strongly on the way the fibres have been placed.The pattern could be in one dimension along a line, or in the two-dimension. Theoretically, the higher dimension LLS model is the best for soil failure modelling, but is inaccurate at solve at practical scales (Hansen *et al.*, 2015).Besides, Sinha *et al.* (2015) proposed that the higher the dimensionality, the smaller the difference between the LLS and ELS. In view of these studies, we choose the ELS as the loading redistribution mechanism.

Sornette (1989) formulated a equation for the calculation of the critical stress at global failure of the bundle, and of the number of broken fibres under a load W with ELS rule. We adopted in our study and incorporated it with the results of infinite slope model, which provide the proportion of broken fires under the driving force. The equation is given as

$$F = P(X_0) - B(\sigma_c - W/N)^{1/2} \tag{12}$$

where F is the proportion of broken fires, P is the CDF for the bundle, $X_0 = k(1/m^{1/m})$, and $B = (mx_0)^{1/2}$ for Weibull distribution. W is the driving fore, and N is the numbers of fires in each soil column. In our numerical solutions, we choose N as 10000, after ensuring any change in N does not significantly alter the model results.

2.3 Flow chart and numerical implementation

A flow chart of the model framework is presented in figure 5. The hydrological analysis was based on the soil property data and rainfall data. Then the infinite slope analysis is conducted with seismic loading of PGA, and the driving force and resisting forces are derived and stored spatially for FBM implementation.

Weibull distribution of fibre strength is a key role in FBM calculation. It does not only reveal the the uncertainty of the soil strength, and also provide a certain ranking of fibre for gradual breaking process modelling. Weibull distributions of soil bundles are represented with shape parameters and scale parameters. The shape parameter is estimated by fractal dimension based on the soil clay content. The scale parameter is estimated by shape parameter, and soil strength from infinite slope analysis.

After representing the soil strength with Weibull distribution, then implement the FBM. since loads are applied on fibers, the first fibre fails, and load redistribution among fibres causes cascade breaking until the bundle of fibre reaches equilibrium or all fibres break.

At last, the FBM provides the percentage of broken fibres for every soil bundle spatially. The percentage of broken fibres ranges from 0 to 100%, and areas with 100% means landslides happen.

The modelling process is performed in the OpenLISEM hazard software, an open-source

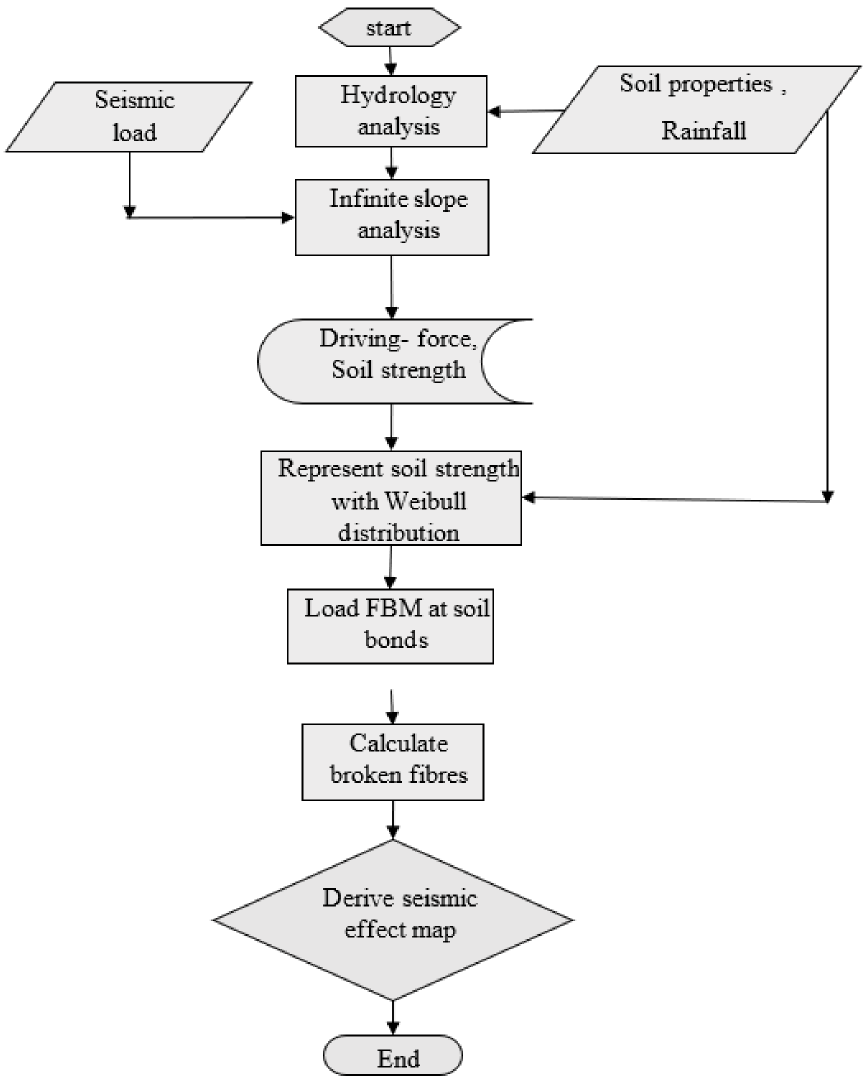

Figure 5: A schematic overview of the model framework conducted in OpenLIESM

geo-spatial modelling tool (Bout *et al.*, 2018). The data input consists of a set of projected rasterized grids, in GeoTIFF for input.

3 Study Case

3.1 Landslides triggered by the 1994 Northridge earthquake

The model was applied to the area affected by the Northridge earthquake ($Mw = 6.7$, January 17, 1994 Northridge, California). This area was chosen because of the availability of data and the possibility to compare the results with earlier work. The earthquake triggered

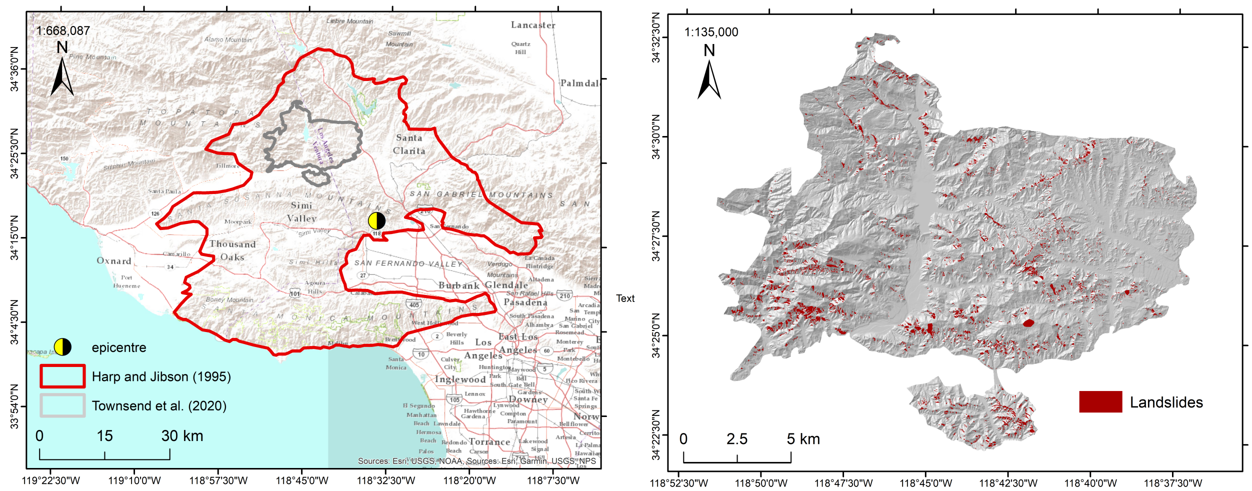

Figure 6: The left is the overview of the study area, the red area was mapped by Harp and Jibson (1995), the grey area was mapped by Townsend *et al.* (2020); The right is the landslide inventory of Townsend *et al.* (2020).

more than 11,000 co-seismic landslides over an area of about 10,000 km², most of them were concentrated in an area of 1000 km² (Jibson *et al.*, 2000)).

There are steep areas, such the Santa Susana Mountains in the north, Oak Ridge in the northwest corner, and the Simi Hills in the south (Parise and Jibson, 2000). For the 1994 earthquake, Jibson *et al.* (1998) indicated that the Arias intensities ranges from 1.14 to 3.92 m/s, which corresponds to PGA between 0.35 and 1.00 g. The earthquakes strength was further evidenced by the large landslides that occured.

An earthquake-induced landslide (EQIL) inventory was made by Harp and Jibson (1995), who manually digitized the landslides mapped on the 1:24,000-scale base maps, after interpreting the landslides from the airphotos. Further co-seismic landslides inventory mapping for this earthquake event was conducted by Townsend *et al.* (2020), for a portion of the Northridge area based on the original inventory (Jibson, 1995), for which they removed the effects of amalgamation, relocated misplaced landslides, and removed anomalously large landslide polygons that contained a mix of disturbed and undisturbed regions. We choose the latest inventory mapped by Townsend *et al.* (2020) for the modelling because of the higher accuracy even though it covers a smaller area (See Figure 6).

3.2 Model Input and Parameters

The input data contained nine variables related to elevation, soil properties and peak ground acceleration (See Table 1 and Figure 7).

Topographic data, particularly recent and very accurate topographic data, are essential to the modelling of landslides, where the Shuttle Radar Topography Mission (SRTM) offers a high-resolution digital elevation (DEM) model with great benefits of homogeneous quality

Base Map	Parameter	Source
Elevation	Pre-Earthquake DTM from SRTM (30 m)	USGS
Soil Material	Soil clay content	USDA
	Internal friction angle	USDA
	Soil cohesion	USDA
	Soil porosity	Estimated through pesudeotranfer function
	ground water height	Modelled through OpenLISEM
	Density	USDA
	Soil depth	Modelled through OpenLISEM
Shake Map	Peak ground acceleration	USGS

Table 1: Spatial input data

and free availability.

Important soil parameters such as soil clay content (soil texture), soil cohesion, and density were obtained from USDA. Other parameters such as Soil porosity, ground water height were estimated using pedotransfer function and using Openlisem software.

Soil depth is defined as the depth of the bedrock interface, which is an essential component of the pattern frame, primarily associated with the driving force W. Due to limited availability of borehole data, soil depth was modelled using OpenLISEM, using the soil evaluation approache from Stothoff (2008).

The ground water height was modelled in OpenLISEM using a steady state depth-average ground water flow model. The initial water content in the soil was set to 0.6, and 2 months of precipitation was simulated to obtain a spatial estimate of soil moisture values. This required the digital terrain map, soil depth, porosity , and water conductivity.

The seismic load input was the horizontal peak acceleration from ShakeMap (Wald *et al.*, 2005), which is a product of the USGS Earthquake Hazards Program in conjunction with the regional seismic networks.

3.3 Calibration and Validation

The coseismic landslide inventory remapped by Townsend *et al.* (2020) contains 5064 landslides. We randomly separated the landslide inventory into two parts for the calibration and validation respectively. The area in the north-west was used for the calibration and contains 3527 landslides, and the remaining 1537 landslides for validation.

The simulations were automated calibrated in the OpenLISEM software, which includes a calibration procedure based on the gradient descent with Armijo-backtracking (Armijo, 1966). This algorithm involves starting with a relatively large estimate of the step size for movement along the search direction,and iteratively shrinking the step size until finding the lowest error. The error is estimated using the Continuous Cohen's kappa score (Sim and

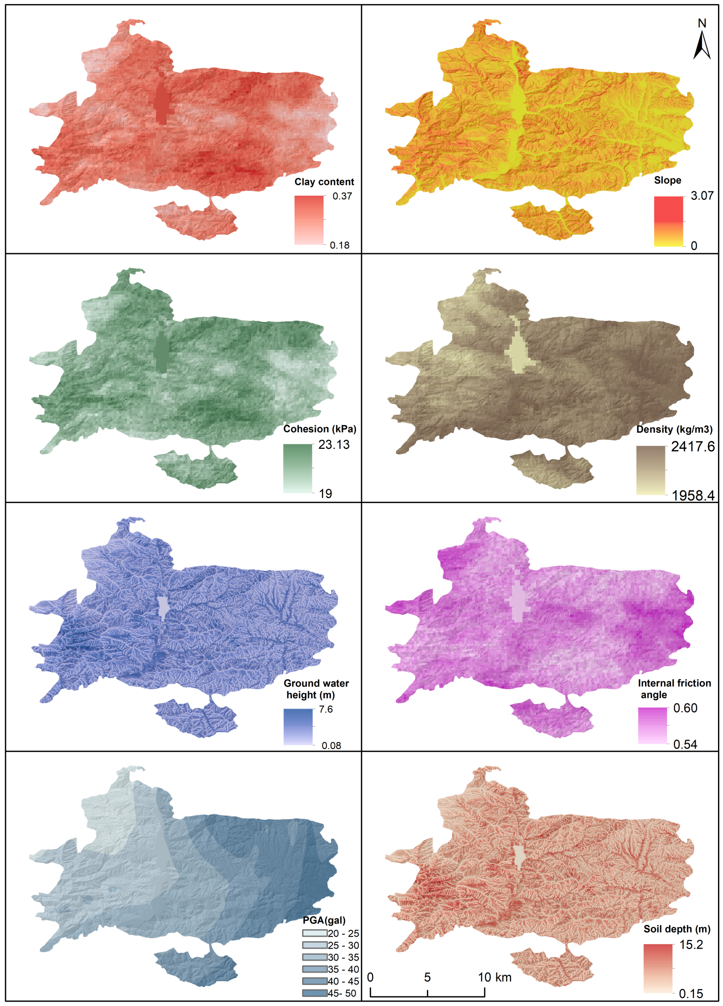

Figure 7: The input layers.

Wright, 2005), which takes into account both correctly predicted positives, negatives, and incorrectly predicted areas.

after calibration, another method used for evaluating the the model accuracy is the receiver operating characteristic curve (ROC curve) (Mandrekar, 2010).The ROC calculates the AUC (Area Under The Curve) as one of the most important metrics for checking the model's performance.

4 Modelling Results and Discussion

Six group of combination of parameters were adopted for calibration with a computing time of twenty minutes. The best calibrated results of was derived with the soil cohesion and internal friction angle with multipliers 0.29 and 1.62 respectively, which gives a Cohen's

Combinations	Varibales	Original Average	Calibrated Multiplier	Cohen's Kappa
1	Soil depth	4.14	0.29	0.225
	Cohesion	21	0.29	
2	Soil depth	4.14	1.81	0.257
	Interal friction angle	0.586	1.43	
3	PGA	34	0.1	0.23
	Cohesion	21	0.86	
4	PGA	34	1.43	0.228
	Interal friction angle	0.568	1.05	
5	Soil depth	4.14	1.24	0.229
	PGA	34	0.1	
6	Cohesion	21	0.29	0.265
	Interal friction angle	0.568	1.62	

Table 2:

Kappa value of 0.265. We used these multipliers conducting the ROC calculation for both calibration and validation areas. Figure 9 shows the accuracy results by using the ROC curve, which gives a calibration accuracy of 0.8416 and a validation accuracy of 0.7383. The final coseismic effect is presented as a damage level range from 0 to 100%, and the 100% damage means landslides triggered (See Figure 10(a)). Figure 10(b) shows the comparison of modelled landslides with landslide inventory. The model provided the internal damage of soil as the index of seismic effect, which is represented as percentage. In order to understand the relationship of the damage level with the landslide triggering, we plotted their distribution (Figure 11). A huge gap between 100% and 34% illustrates that when soil columns reach the threshold damage level of about 34%, the whole soil column would fail suddenly.

The calibration with Cohen's kappa gave a coefficient of 0.96 with the multipliers of 0.29 for soil depth, and of 1.05 for soil cohesion. We used these multipliers conducting the ROC calculation. Figure 8 shows the accuracy results by using the ROC curve, which gives a calibration accuracy of 0.8419 and a validation accuracy of 0.7678.

The final coseismic effect is presented as a damage level range from 0 to 100%, and the 100% damage means landslides triggered (See Figure 9(a)). Figure 9(b) shows the comparison of modelled landslides with landslide inventory.

The model provided the internal damage of soil as the index of seismic effect, which is represented as percentage. In order to understand the relationship of the damage level with the landslide triggering, we plotted their distribution (Figure 10). A lack of fractional damage values between 100% and 34% illustrates that when soil columns reach the threshold damage level of about 34%, the whole soil column would fail suddenly due to catastrophic load redistribution.

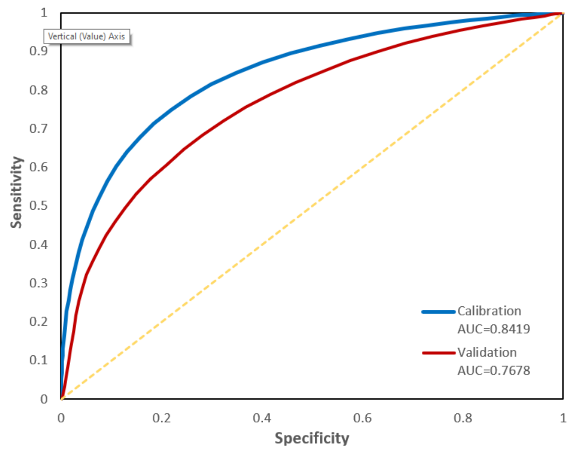

Figure 8: The ROC curves for the calibration and validation areas

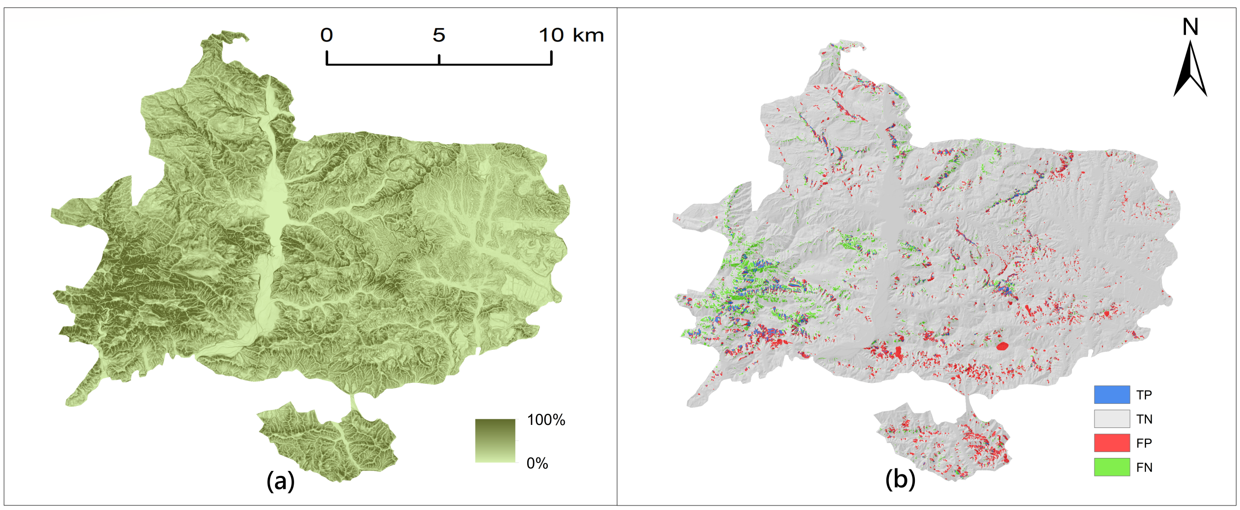

Figure 9: A comparison of the simulation results map and the landslide inventory

4.1 Internal damage

For the non-landslide slopes, the distribution between 0% to 34% shows the a positive skewness. The feature tell that these slopes with damage level near the threshold (34%) would more easily developed into landslides with a relative smaller disturbance because they just have fewer remaining soil strength. So these parts area could have a high potential of landslide initiation in sequence events, such as rainfall, snow melting. The internal damage index is a good predictor for post-seismic landslide prediction within both statistic and physically-based models. For statistical modelling, the index could be used as an important co-variate for landslide prediction in post-seismic events. For the physically-based model, it could be used to quantify the loss of the soil strength by integrating the residual strength after breaking, the subsequent soil healing, and the root strengthening. What cannot be ignored is

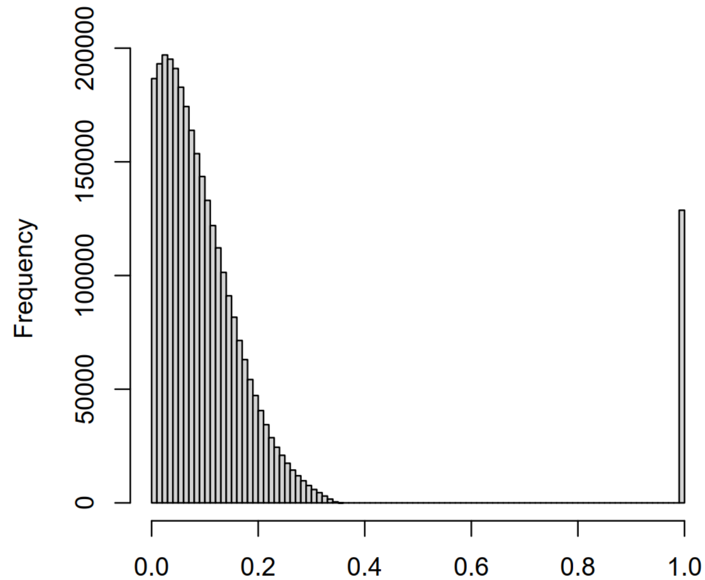

Figure 10: The distribution of the internal damage.

that the index of landslide area and deposit area should be adjusted based on the new soil on slopes. The fractional damage has a further link with the probability of failure. Our implementation of the fibre bundle framework applies slope stability equations to a PDF of potential fibre strengths. This PDF is chosen carefully to reflect the likely range of values. As such, the model acts analogously to monte-carlo simulation of slope stability. The fractional internal damage reflects the percentage of possible strength parameter values that result in failure after application of the model. A critical difference to the presented work is the global load redistribution after partial damage.

4.2 Missing Gap

Within the simulation outcomes, the slopes internal damage is distributed completely on the range [0%,34%] and 100%.

The absence of slope with damages between 34% and 100% are related to the underlying theory. Due to the load redistribution and the selected PDF for shear capacity, any damage above 34% will result in such high loads on the other fibers that the catastrophic point is reached. The total force cannot be held by the remaining fibres and total failure occurs. The physical process similarly features a distinction in the mobilization processes of sloping rocks and soil under seismic loads. The term “mobilization” in a general sense includes both fracture and flow. The fracture implies the appearance of distinct surfaces of separation in the body of soil, whereas the flow features the yield of plastic-elastic behavior, which is the onset of plastic deformation (Young, 2012).

The missing values between 34% and 100% damage, indicate two triggering mechanism among co-seismic landslides based on the rule of load redistribution. The first one is gradual, potentially failing landslides. These locations can feature significant damage, obtained during the seismic shaking. However, they did not abruptly fail, and might progress to full failure later during aftershocks or due to hydrological triggers. The second one is directly shearing landslides, which caused by the relatively fast and direct impacts from the ground shaking. The gradual yield and direct impact may present different moving features.The phenomena could be the specific performances of the soil characteristics of elastic, plastic, and brittle. From the model results, it can be observed that besides directly failing slopes, vast areas are near critical damage. The effects of this, often called seismic legacy effects in literature, can be estimated with this method. The discovery may give us a new insight to classify the co-seismic landslides into more detailed subdivisions with different triggering mechanisms and estimate increase in susceptibility.

4.3 Slope failure

The resulting slope failure pattern shows a generally good match with the landslide inventory. It does provide confidence in the pattern predicted by the method. However, some modelling results (Figure 9) in the western part of the study area are larger than the actual landslides in inventory, while the opposite is true in the eastern part. In order to explore this further, we overlaid the variables on the modelling results, and found this bias is related to the PGA. In the east with higher PGA, there are more false positive points, while in the west, there are more false negative. Our model could overestimate seismic effect for areas with high PGA, and underestimate it for areas with low PGA. One possible reason is that PGA map itself is a simplification of seismic effect. This should further motivate the field of landslide science that seismic time history data would have potential for improving predictions.

4.4 Reclassification of Seismic Effect

The initial earthquake damage on slope are divided into four groups (See Figure 1). However, the results gives us a more detail solution for further modelling.

First of all, seismic load could just cause intern damage, and also could be directly sheared. Second, damaged slopes could develop to landslide suddenly within a certain ground motion, and also could evolve to failure through load redistribution. Thus, there are five situations for slopes under ground shaking. Current, our model cannot distinguish the gradually failure and directly shearing landslides because of lack of a specific data in Northridge area. In the further work, this is would be a critical point to discover.

4.5 Uncertainties of Soil properties

The uncertainty quantification of soil properties is worthy to study for physically-based modelling, because thus we could improve the modelling accuracy and figure out the defects of data for further improvement. Many reasons could cause uncertainty, such as lack of information about the randomness of the object, unknown accuracies of available information,

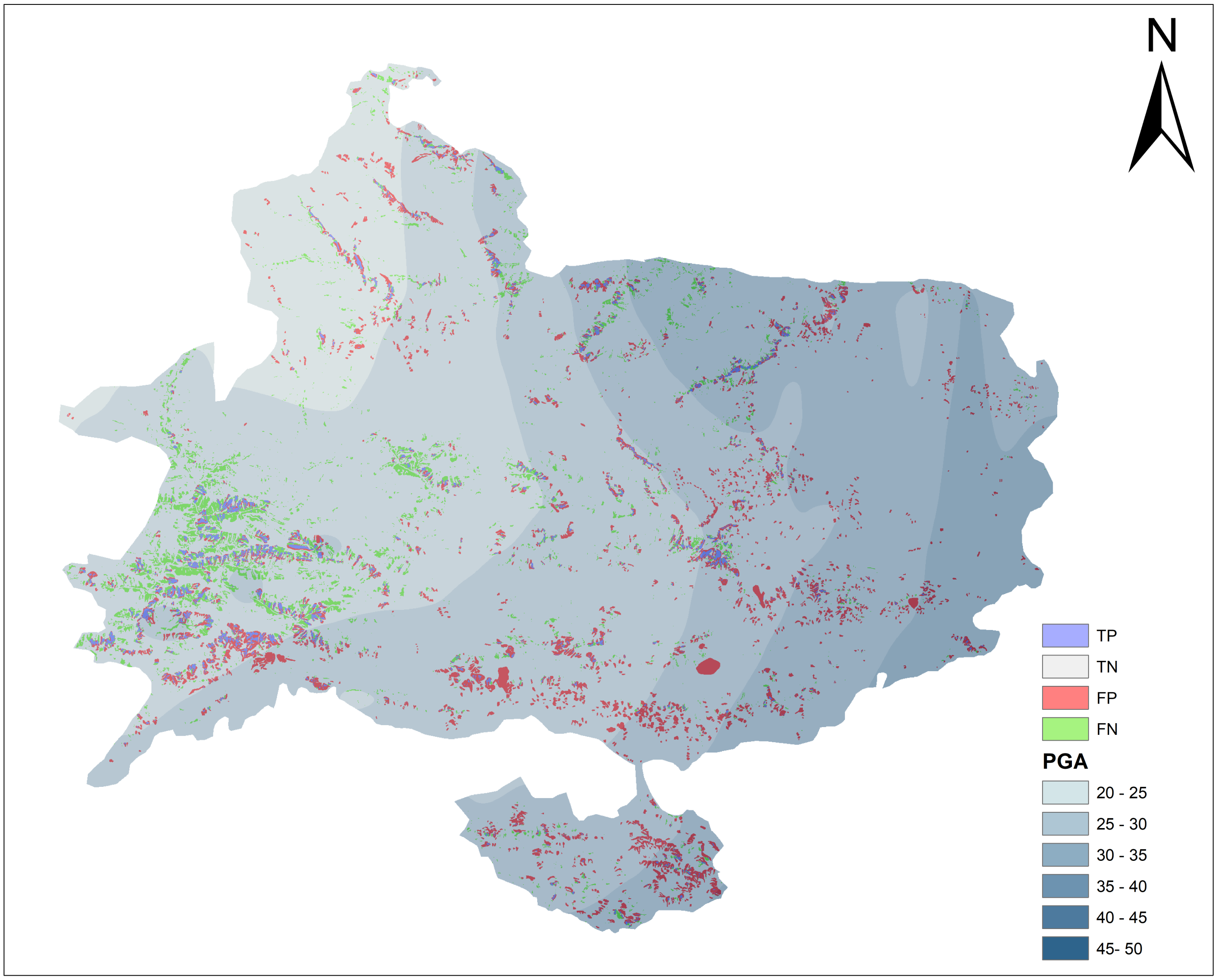

Figure 11: The comparison of the resulting landslides with PAG map

lack of technology to acquire needed information, and impossibility of making essential measurements, etc (Rao *et al.*, 1989). For the soil properties, each property has its characteristic of uncertainty, which differ in the ranges and the leading reasons. For example, the soil density is mainly depending on the accuracy of measurement, while the soil cohesion is not only depending on the measurement, but also depending on the interactions of the various constituents and micro structures of soil-water system, which define the integrity of the soil system (Young, 2012).

The Weibull distribution of soil shear strength is a specific presentation of the second uncertainty (Figure 13). As we all know, the determination of the shearing strength can be obtained through lab test, which associated with many fundamental factors, such as the test system, strain or stress-controlled load application, stress and strain history, temperature, soil fabric, density, saturation, water content, etc (Graham *et al.*, 1983). These factors are difficult to be controlled and evaluated, thus would producing uncertainty for the soil resistance.

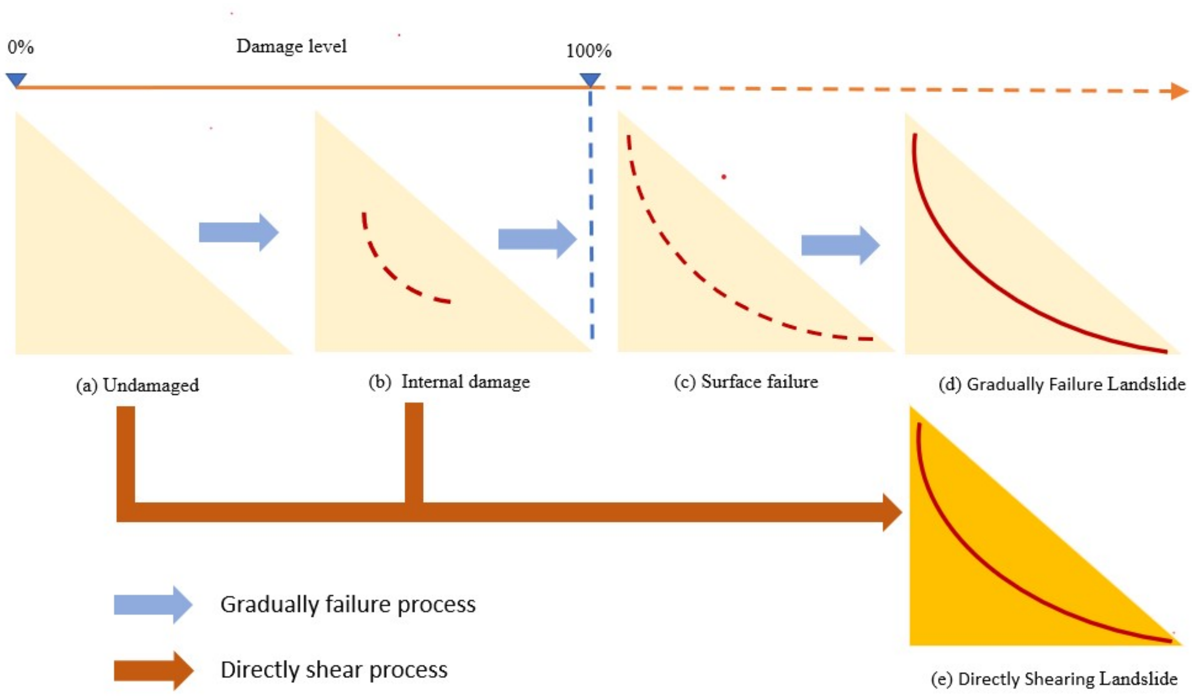

Figure 12: The reclassification of seismic effect on slopes.

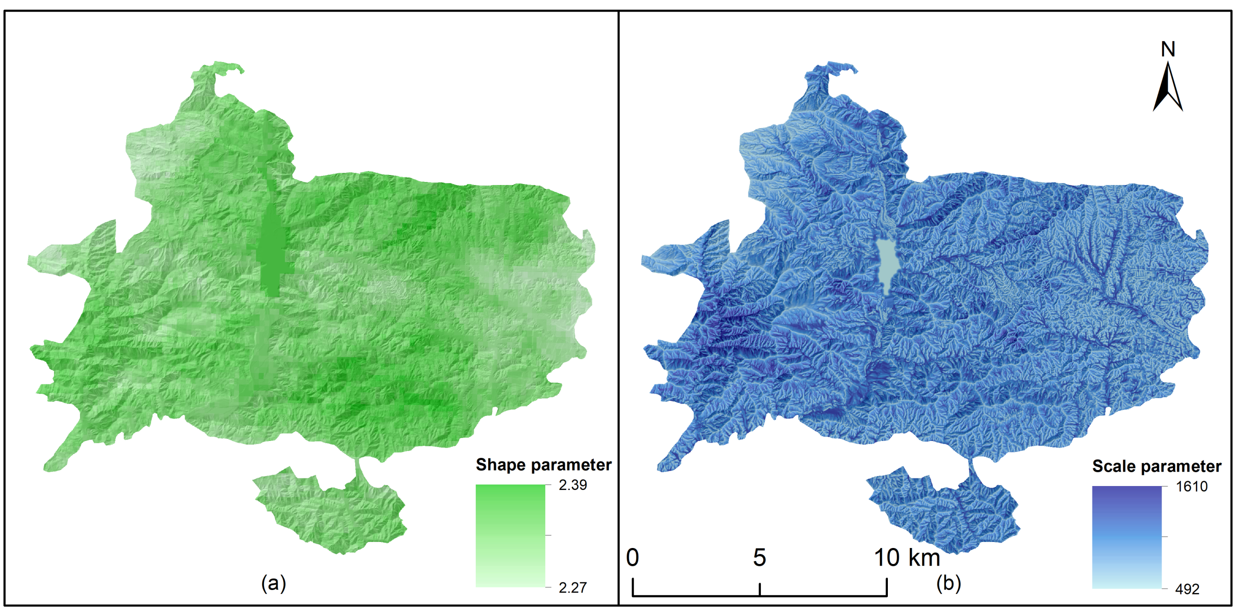

Figure 13: The spatial values of the Weibull parameter m (left) and k (right).

While the Mohor-Coulomb criterion provided a effective analytic solution pertaining to the cohesion c, internal friction angle ϕ and normal stress σ. However, it may not necessary revel the actual soil response behaviour, so the mechanistic interpretation of c and ϕ are still unclear. So the probability presentation of soil shear strength is salient for evaluating our uncertainty about the complex system. The Weibull distribution shape parameters m derived form the soil texture successfully gives estimation of uncertainty, and the scale parameter k limits the domain of strength values. This method integrated into FBM, offer a well expected failure result which involves the complexity of soil system. With the more and deeper understanding we get about soil, the probability distribution of soil strength would become more centralized, thus the physically-based model would become robuster.

5 Conclusions

This physically based model provides a useful tool to quantify the seismic effects on hillslopes. During the 1994 extreme earthquake event in Northridge area, thousands of landslides were initiated by the ground shaking, as the shear strength of the sloping materials was overcome by seismic loads. Our developed modeling approach allowed for quantification of the earthquake impact. The model simulated the hazardous landslide areas prone to either failure, or that obtained some fractional damage, expressed as the fraction of broken fibers. This fractional damage shows potential for interpretation in indirect failures triggered after an earthquake. Further more, the modelling results demonstrated the thresholds of damage level for landslide initiation, which offer us a new insight for sloe stability analysis in the aspect of nonlinear failure. Using the model that integrates shallow landslide and damage level, can thus increase the accuracy of hazard and risk assessment.

Lack of available data limits the predictions of the spatial location of slope failure and estimation of soil damage. Further more, the model does not differentiate the landslide triggering area and runout area due to the lack of classification of them in landslide inventory. So, the model would overrate the landslide areas during the calibration. In order to solve this problem, more detailed and small scale landslide inventory could be adopted for future improvement of this model. More over, this model do not consider the interaction processes among failed soil columns themselves, and unfailed soil columns. Once a soil column fails, it would change the mechanical situation with its neighbour soil columns by transporting compressive stress and tensile stress. This phenomenon could cause cascading failure downward and upward. At last, even though PGA is eligible to represent the earthquake force on slopes, it actually simplifies the temporally dynamic process of seismic load on slopes into a constant, and thus it can not reveal the dynamic process of failure during ground shaking fully. Detailed seismic observations or spatial modelling results must be investigated further.

6 Acknowledgements

In addition, we would like to thank Hakan Tanyas and Ashok Dahal for their work and support on the landslide inventories.

7 Code Availability

Nem of the code/library Contact: FBM-Seismic model, Yuanjing Chen (y.chen-6@utwente.nl). Hardware Requirements: NA. Programming Language: LISEM Script Program Size: 150 lines Software Required: LISEM (www.lisemmodel.com) The source codes are available under GPL-3 licence, and hosted on github ($https : //github.com/CYJZJCS/FBM_Seismic-$).

8 Code Availability

The data used in this article are available on request through the DANS repository (Pending).

9 Declaration of competing interests

The authors declare that they have no knowm competing financial interests or personal relationships that could have appeared to influence the work reported in this paper.

A Appendix: Estimation of Fractal dimension

The fractal dimension is strongly correlated with soil texture. The studies from Tyler and Wheatcraft (1992); Bittelli *et al.* (1999); Huang and Zhang (2005) showed that the fractal dimension increases with the increase in clay content and decreases with the sand content. Huang and Zhang (2005) conducted a set of lab experiments to analyse the relationship of fractal dimension with the soil clay content, and used nonlinear fitting procedure proposing the following equation with $r^2 = 0.914$

$$D = a_o + \frac{1 - e^{a_1 C}}{a_2(1 + e^{a_1 C}) + a_3(1 + e^{a_1 C})} \tag{13}$$

where C is the soil clay content, a_0, a_1,a_2, and a_3 are fitted parameters.a_0 equals to 2.05, a_1 equals to 4.39×10^{-3}, a_2 equals to -1.18×10^{-2}, and a_3 equals to 1.10.

References

Abdassah, D., Permadi, P., Sumantri, Y. and Sumantri, R. (1996) Saturation exponents derived from fractal modeling of thin-sections. In *SPE Asia Pacific Oil and Gas Conference.*

Armijo, L. (1966) Minimization of functions having lipschitz continuous first partial derivatives. *Pacific Journal of mathematics* **16**(1), 1–3.

Bishop, A. W. (1959) The principle of effective stress. *Teknisk ukeblad* **39**, 859–863.

Bittelli, M., Campbell, G. S. and Flury, M. (1999) Characterization of particle-size distribution in soils with a fragmentation model. *Soil Science Society of America Journal* **63**(4), 782–788.

Bout, B., Lombardo, L., van Westen, C. J. and Jetten, V. G. (2018) Integration of two-phase solid fluid equations in a catchment model for flashfloods, debris flows and shallow slope failures. *Environmental Modelling & Software* **105**, 1–16.

Brooks, R. H. and Corey, A. T. (1964) Hydraulic properties of porous media and their relation to drainage design. *Transactions of the ASAE* **7**(1), 26–0028.

Cao, W. and Zhang, S. (2005) Research on statistical analysis method of rock damage based on mohr-coulomb criterion. *Journal of Hunan University (Natural Science)* **32**(1), 43–47.

Cohen, D., Lehmann, P. and Or, D. (2009) Fiber bundle model for multiscale modeling of hydromechanical triggering of shallow landslides. *Water resources research* **45**(10).

Fan, L., Lehmann, P. and Or, D. (2015) Effects of hydromechanical loading history and antecedent soil mechanical damage on shallow landslide triggering. *Journal of Geophysical Research: Earth Surface* **120**(10), 1990–2015.

Fan, L., Lehmann, P. and Or, D. (2016) Effects of soil spatial variability at the hillslope and catchment scales on characteristics of rainfall-induced landslides. *Water Resources Research* **52**(3), 1781–1799.

Fan, X., Scaringi, G., Korup, O., West, A. J., van Westen, C. J., Tanyas, H., Hovius, N., Hales, T. C., Jibson, R. W., Allstadt, K. E. *et al.* (2019) Earthquake-induced chains of geologic hazards: Patterns, mechanisms, and impacts. *Reviews of geophysics* **57**(2), 421–503.

Friesen, W. and Mikula, R. (1987) Fractal dimensions of coal particles. *Journal of Colloid and Interface Science* **120**(1), 263–271.

Galambos, J. (1978) The asymptotic theory of extreme order statistics. Technical report.

Gao F, X. H. P. (1996) Statistically fractal strength theory for brittle materials. *Acta Mechanica Solida Sinica* **17**(3), 239–245.

Graham, J., Crooks, J. and Bell, A. L. (1983) Time effects on the stress-strain behaviour of natural soft clays. *Géotechnique* **33**(3), 327–340.

Hansen, A., Hemmer, P. C. and Pradhan, S. (2015) *The fiber bundle model: modeling failure in materials*. John Wiley & Sons.

Harp, E. L. and Jibson, R. W. (1995) Seismic instrumentation of landslides: Building a better model of dynamic landslide behavior. *Bulletin of the Seismological Society of America* **85**(1), 93–99.

Huang, G. and Zhang, R. (2005) Evaluation of soil water retention curve with the pore–solid fractal model. *Geoderma* **127**(1-2), 52–61.

Ingles, J., Darrozes, J. and Soula, J.-C. (2006) Effects of the vertical component of ground shaking on earthquake-induced landslide displacements using generalized newmark analysis. *Engineering geology* **86**(2-3), 134–147.

Jibson, E. L. H. R. W. (1995) Inventory of landslides triggered by the 1994 northridge, california earthquake .

Jibson, R. W. (2007) Regression models for estimating coseismic landslide displacement. *Engineering geology* **91**(2-4), 209–218.

Jibson, R. W., Harp, E. L. and Michael, J. A. (1998) *A method for producing digital probabilistic seismic landslide hazard maps: an example from the Los Angeles, California, area.* Citeseer.

Jibson, R. W., Harp, E. L. and Michael, J. A. (2000) A method for producing digital probabilistic seismic landslide hazard maps. *Engineering geology* **58**(3-4), 271–289.

Kewen, L. (2004) Theoretical development of the brooks-corey capillary pressure model from fractal modeling of porous media. In *SPE/DOE Symposium on Improved Oil Recovery.*

Lari, S., Frattini, P. and Crosta, G. (2014) A probabilistic approach for landslide hazard analysis. *Engineering geology* **182**, 3–14.

Lehmann, P. and Or, D. (2012) Hydromechanical triggering of landslides: From progressive local failures to mass release. *Water Resources Research* **48**(3).

Leshchinsky, B., Lehmann, P. and Or, D. (2021) Enhanced rainfall-induced shallow landslide activity following seismic disturbance—from triggering to healing. *Journal of Geophysical Research: Earth Surface* **126**(1), e2020JF005669.

Lim, W. L., McDowell, G. R. and Collop, A. C. (2004) The application of weibull statistics to the strength of railway ballast. *Granular Matter* **6**(4), 229–237.

Lombardo, L. and Mai, P. M. (2018) Presenting logistic regression-based landslide susceptibility results. *Engineering geology* **244**, 14–24.

Lu, N., Godt, J. W. and Wu, D. T. (2010) A closed-form equation for effective stress in unsaturated soil. *Water Resources Research* **46**(5).

Mandrekar, J. N. (2010) Receiver operating characteristic curve in diagnostic test assessment. *Journal of Thoracic Oncology* **5**(9), 1315–1316.

Marc, O., Meunier, P. and Hovius, N. (2017) Prediction of the area affected by earthquake-induced landsliding based on seismological parameters. *Natural Hazards and Earth System Sciences* **17**(7), 1159–1175.

Meunier, P., Hovius, N. and Haines, A. J. (2007) Regional patterns of earthquake-triggered landslides and their relation to ground motion. *Geophysical Research Letters* **34**(20).

Meunier, P., Hovius, N. and Haines, J. A. (2008) Topographic site effects and the location of earthquake induced landslides. *Earth and Planetary Science Letters* **275**(3-4), 221–232.

Morgenstern, N. and Sangrey, D. A. (1978) Methods of stability analysis. *Transportation Research Board Special Report* (176).

Munkholm, L. and Perfect, E. (2005) Brittle fracture of soil aggregates: Weibull models and methods of parameter estimation. *Soil Science Society of America Journal* **69**(5), 1565–1571.

Munkholm, L. J., Perfect, E. and Grove, J. (2007) Incorporation of water content in the weibull model for soil aggregate strength. *Soil Science Society of America Journal* **71**(3), 682–691.

Newmark, N. M. (1965) Effects of earthquakes on dams and embankments. *Geotechnique* **15**(2), 139–160.

Parise, M. and Jibson, R. W. (2000) A seismic landslide susceptibility rating of geologic units based on analysis of characteristics of landslides triggered by the 17 january, 1994 northridge, california earthquake. *Engineering geology* **58**(3-4), 251–270.

Peirce, F. T. (1926) Tensile tests for cotton yarns: "the weakest link" theorems on the strength of long and of composite specimens. *J. Textile Inst* **17**, T355–368.

Rao, C. R. *et al.* (1989) Statistics and truth. *Putting Chance to Work* .

Reichenbach, P., Rossi, M., Malamud, B. D., Mihir, M. and Guzzetti, F. (2018) A review of statistically-based landslide susceptibility models. *Earth-science reviews* **180**, 60–91.

Reid, M. E., Christian, S. B., Brien, D. L. and Henderson, S. (2015) Scoops3d—software to analyze three-dimensional slope stability throughout a digital landscape. *US Geological Survey Techniques and Methods, book* **14**.

Rinne, H. (2008) *The Weibull distribution: a handbook*. Chapman and Hall/CRC.

von Ruette, J., Lehmann, P. and Or, D. (2013) Rainfall-triggered shallow landslides at catchment scale: Threshold mechanics-based modeling for abruptness and localization. *Water Resources Research* **49**(10), 6266–6285.

Shen, P. and Li, K. (1994) A new method for determining the fractal dimension of pore structures and its application. In *Proceedings of the 10th Offshore South East Asia Conference, Singapore*, pp. 6–9.

Shen, P., Li, K. and Jia, F. (1995) Quantitative description for the heterogeneity of pore structure by using mercury capillary pressure curves. In *International Meeting on Petroleum Engineering*.

Sim, J. and Wright, C. C. (2005) The kappa statistic in reliability studies: use, interpretation, and sample size requirements. *Physical therapy* **85**(3), 257–268.

Sinha, S., Kjellstadli, J. T. and Hansen, A. (2015) Local load-sharing fiber bundle model in higher dimensions. *Physical Review E* **92**(2), 020401.

Sornette, D. (1989) Elasticity and failure of a set of elements loaded in parallel. *Journal of Physics A: Mathematical and General* **22**(6), L243.

Stothoff, S. (2008) Infiltration tabulator for yucca mountain: Bases and confirmation. *Prepared for USNRC http://pbadupws. nrc. gov/docs/ML0823/ML082350701. html* .

Süzen, M. L. and Doyuran, V. (2004) A comparison of the gis based landslide susceptibility assessment methods: multivariate versus bivariate. *Environmental geology* **45**(5), 665–679.

Tanyaş, H., Van Westen, C. J., Allstadt, K. E., Anna Nowicki Jessee, M., Görüm, T., Jibson, R. W., Godt, J. W., Sato, H. P., Schmitt, R. G., Marc, O. *et al.* (2017) Presentation and analysis of a worldwide database of earthquake-induced landslide inventories. *Journal of Geophysical Research: Earth Surface* **122**(10), 1991–2015.

Toledo, P. G., Ted Davis, H. and Scriven, L. (1993) Capillary hyperdisperson of wetting liquids in fractal porous media. *Transport in porous media* **10**(1), 81–94.

Townsend, K. F., Gallen, S. F. and Clark, M. K. (2020) Quantifying near-surface rock strength on a regional scale from hillslope stability models. *Journal of Geophysical Research: Earth Surface* **125**(7), e2020JF005665.

Tyler, S. W. and Wheatcraft, S. W. (1992) Fractal scaling of soil particle-size distributions: Analysis and limitations. *Soil Science Society of America Journal* **56**(2), 362–369.

Valagussa, A., Marc, O., Frattini, P. and Crosta, G. (2019) Seismic and geological controls on earthquake-induced landslide size. *Earth and Planetary Science Letters* **506**, 268–281.

Van Westen, C. J., Castellanos, E. and Kuriakose, S. L. (2008) Spatial data for landslide susceptibility, hazard, and vulnerability assessment: An overview. *Engineering geology* **102**(3-4), 112–131.

Wald, D. J., Worden, B. C., Quitoriano, V. and Pankow, K. L. (2005) Shakemap manual: technical manual, user's guide, and software guide. Technical report.

Weibull, W. (2013) *Fatigue testing and analysis of results.* Elsevier.

Xu, C., Xu, X., Yao, X. and Dai, F. (2014) Three (nearly) complete inventories of landslides triggered by the may 12, 2008 wenchuan mw 7.9 earthquake of china and their spatial distribution statistical analysis. *Landslides* **11**(3), 441–461.

Xu, Y., Song, D. and Chu, F. (2016) Approach to the weibull modulus based on fractal fragmentation of particles. *Powder Technology* **292**, 99–107.

Young, R. (2012) *Soil properties and behaviour.* Volume 5. Elsevier.